Eur. Phys. J. D **20**, 357–367 (2002)
DOI: 10.1140/epjd/e2002-00158-3

THE EUROPEAN PHYSICAL JOURNAL D

Electronic excitation and singlet-triplet coupling in uracil tautomers and uracil-water complexes

A quantum chemical investigation

C.M. Marian[a], F. Schneider, M. Kleinschmidt, and J. Tatchen

Institute of Theoretical Chemistry, Heinrich-Heine-University, Universitätsstr. 1, 40225 Düsseldorf, Germany

Received 18 February 2002 / Received in final form 5 June 2002
Published online 13 September 2002 –

Abstract. Electronic spectra of uracil in its diketo (lactam) form and five enol (lactim) tautomeric forms have been investigated by means of combined density functional and configuration interaction methods. We have simulated the effects of hydrogen bonding with a protic solvent by recomputing the spectrum of uracil in the presence of two, four, or six water molecules. Geometries of the electronic ground state and several low-lying excited states have been optimized. Spin-orbit coupling has been determined for correlated wavefunctions employing a non-empirical spin-orbit mean-field approach. In accord with experiment, we find the diketo tautomer to be the most stable one. The calculations confirm that the first absorption band arises from the $^1(\pi \rightarrow \pi^*)$ $S_0 \rightarrow S_2$ excitation. The experimentally observed vibrational structure in this band originates from a breathing mode of the six ring. Complexation with water molecules is seen to cause a significant blue shift of $n \rightarrow \pi^*$ excitations while leaving $\pi \rightarrow \pi^*$ excitations nearly uninfluenced. Computed radiative lifetimes are presented for the experimentally known weak phosphorescence from the $\pi \rightarrow \pi^*$ excited T_1 state. Among the uracil lactim tautomers, one is particularly interesting from a spectroscopic point of view. In this tautomer, the $\pi \rightarrow \pi^*$ excitation gives rise to the S_1 state.

PACS. 31. Electronic structure of atoms and molecules: theory – 33. Molecular properties and interaction with photons – 33.50.-j Fluorescence and phosphorescence; radiationless transitions, quenching (intersystem crossing, internal conversion)

1 Introduction

The pyrimidine bases uracil and thymine exhibit broad absorption bands in the ultra violet, both in the gas phase and in solution [1–7]. The first band with an onset at approximately 4.5 eV in vapor spectra has been assigned to a $\pi \rightarrow \pi^*$ transition [2,7]. This assignment is supported by recent *ab initio* quantum chemical studies [8,9]. They have shown that the $\pi \rightarrow \pi^*$ excited S_2 states of uracil and thymine are the lowest singlet states connected with the S_0 ground state by a considerable dipole transition probability. The computed oscillator strength for the $n \rightarrow \pi^*$ transition ($S_0 \rightarrow S_1$) is about three orders of magnitude smaller. In the first system, some vibrational structure was resolved (uracil $\approx$ 790 cm^{-1}; thymine $\approx$ 740 cm^{-1} at low temperatures (77 K) in 2-methyltetrahydrofuran (2-MTHF)) [3]. At room temperature or in methanol-ethanol, no vibrational structure could be made out. Further, Becker and Kogan report weak fluorescence or phosphorescence, the appearance of which depends strongly on the solvent.

The reason for the diffuseness of the absorption spectra of thymine and uracil is not yet clear. Brady *et al.* attribute the spectral broadening either to mixing with a lower-lying electronic state or to a large geometry change between the ground and excited electronic states [7]. Candidates for an extensive intensity borrowing from the S_2 state of uracil could be highly excited vibronic levels of S_0, S_1, or some triplet state. High quality *ab initio* investigations predict S_1 to have a vertical excitation energy of about 4.5 eV [9], just at the onset of the observed broad band. So far, the energetic location of the triplet states has not been determined with high confidence and knowledge about electronic singlet-triplet coupling strengths in uracil is completely missing. Considering geometric effects, certainly a change of bond lengths and angles is to be expected upon a $\pi \rightarrow \pi^*$ excitation. It is not known, however, how strongly the molecular geometry influences the electronic spectrum.

Due to hydrogen migration, several tautomeric forms of uracil can be thought of (*cf.* Fig. 1). It is generally agreed that the diketo (lactam) form (A) is the most stable one in the electronic ground state and no other tautomer has ever been identified in solution or in the gas phase [3].

[a] e-mail: Christel.Marian@uni-duesseldorf.de

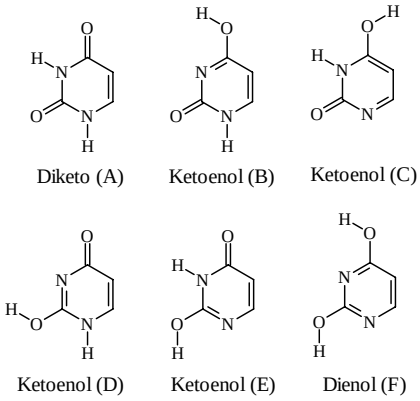

Fig. 1. Six tautomeric forms of uracil.

The situation is less clear for the excited electronic states, however. Ito and coworkers reported two band systems with well-resolved vibrational structures in fluorescence excitation and dispersed fluorescence spectra in a supersonic jet [5,6]. They assigned the two band systems with 0^0 transition wavenumbers of 35 288 cm^{-1} (4.38 eV, system I) and 30 917 cm^{-1} (3.83 eV, system II) to $n \rightarrow \pi^*$ transitions in the diketo and a ketoenol tautomer, respectively. If the observation of a ketoenol tautomer of uracil or thymine were confirmed, this had large implications with respect to mutations in RNA or DNA replication. Brady *et al.* were able to reproduce system I [7]. They could show, however, that the carrier of this sharp fluorescence spectrum was not uracil but an impurity with higher mass produced in the oven. The origin of system II remained unclear.

The aim of the present quantum chemical study is to find an answer to some of these open questions. For all six tautomers shown in Figure 1, we have determined the ground state geometry and the electronic spectrum as well as properties of the low-lying singlet and triplet states including their spin-orbit interaction. We have studied the effects of singlet and triplet $\pi \rightarrow \pi^*$ and $n \rightarrow \pi^*$ excitations on the geometry of the diketo tautomeric form. The geometry relaxation after $\pi \rightarrow \sigma^*$ excitations has been estimated by calculating the electronic spectrum at the optimized geometry of the corresponding triplet state, T_4. Further, we have investigated the influence of hydrogen bonding on the molecular structure and the electronic spectrum by computing several uracil water complexes.

2 Methods

The reliable quantum chemical evaluation of the electronic spectrum and the spin-orbit coupling between electronic states requires the inclusion of static and dynamic electron correlation in the wavefunction determination as well as an efficient treatment of spin-orbit coupling. Standard *ab initio* packages are not applicable for this purpose, if the number of correlated electrons is large.

The combined density functional theory/multi-reference configuration interaction (DFT/MRCI) method by Grimme and Waletzke has proven to yield excellent electronic spectra of organic molecules [10]. We have used this method for the determination of pure singlet and triplet electronic states of uracil in various tautomeric forms. The idea behind this approach is to include major parts of dynamic electron correlation by density functional theory whereas short MRCI expansions take account of static correlation effects. To this end, the configuration state functions (CSFs) in the MRCI expansion are built up from Kohn-Sham (KS) orbitals. Diagonal elements of the effective DFT/MRCI Hamiltonian are constructed from the corresponding Hartree-Fock based expression and a DFT specific correction term. In the effective DFT/MRCI Hamiltonian, all in all five empirical parameters are employed. These parameters depend only on the multiplicity of the desired state, the number of open shells of a configuration, and the employed density functional, but not on the specific atom or molecule. Currently, optimized parameter sets are available only for singlet and triplet multiplicities in combination with the BH-LYP [11,12] functional. A common set of reference CSFs is used for all spatial symmetries. The initial set can be generated automatically in a complete active space (CAS)-like procedure and is then iteratively improved. The MRCI expansion is kept short by extensive configuration selection. For further details, we refer to the original publication by Grimme and Waletzke [10].

Technically, the MRCI code and the associated property programs are linked to the Turbomole package [13,14]. They can thus take advantage of the efficiency with which the latter determines two-electron integrals and KS wavefunctions even for large molecules. Computationally expensive four-index integrals are evaluated using the well-known resolution of the identity (RI) method employing the RI-MP2 optimized auxiliary basis sets from the Turbomole library [15–17].

Geometry optimizations at the (U)DFT level were performed utilizing analytical gradients and approximate Hessians as generated by the rdgrad and relax modules of the Turbomole package. Unfortunately, these methods cannot be applied to open-shell singlet states. Moreover, analytical DFT/MRCI gradients are not yet available. To enable the geometry optimization of the S_1 and S_2 states at the correlated level, gradients were constructed numerically by finite difference techniques and the minima were located by a conjugate gradient search [18]. The current first program version works sequentially (one energy point at a time) and includes drivers for the dscf and ridft modules of Turbomole and for a DFT/MRCI calculation. An improved parallelized version will be available soon.

Spin-orbit matrix elements for DFT/MRCI wavefunctions have been generated with the recently presented spin-orbit coupling kit (Spock) [19]. Key features of this program are a fast determination of spin-coupling coefficients between CSFs for spin-dependent one-electron operators and the use of non-empirical atomic spin-orbit mean-field integrals. The spin-orbit mean-field Hamiltonian utilized in this work is an effective one-electron operator derived from the Breit-Pauli Hamiltonian; herein,

screening by other electrons is incorporated in a Fock-like manner [20]. As an additional approximation, all multi-center spin-orbit integrals are neglected. In this way, the molecular mean field reduces to a sum of atomic mean fields.

The spin-orbit mean-field approach as such was shown to yield matrix elements in excellent agreement with those of the full one- and two-electron spin-orbit Hamiltonian [20]. Even for light molecules, the errors are usually well below 1% [21,22]. For light, conjugated molecules such as uracil, the one-center approximation is the most critical one in the hierarchy of approximations for the treatment of spin-orbit coupling. It was originally developed for the treatment of spin-orbit coupling in heavy metal compounds [20]. Multi-center spin-orbit integrals were found to contribute approximately 5% to the spin-orbit splitting in the ground state of the π-conjugated molecules HC_6H^+, NC_5H^+, and NC_4N^+, composed of first-row elements only [21]. Errors of this size appear acceptable, as a full spin-orbit treatment is presently out of reach for molecules of the size of uracil. Moreover, there are little alternatives to this procedure. A neglect of multi-center two-electron integrals only, while keeping all generic one-electron terms, leads to larger deviations because the one- and two-electron multi-center terms tend to cancel systematically. Pseudopotential approaches that are technically also feasible meet the very same difficulties as the mean-field approach whereas parameterized effective charge spin-orbit Hamiltonians are generally too crude.

Spock is interfaced to the Turbomole package by the program SOmf [19]. Herein, mean-field orbitals are generated automatically for each atom from a restricted (open-shell) Hartree-Fock atomic ground state calculation and the atomic mean-field integral program Amfi [23] is called. Amfi makes use of spherical symmetry; spin-orbit integral evaluation is thus extremely fast. Finally, SOmf performs the transformation of the spin-orbit integrals from the atomic to the molecular orbital (MO) basis set. The application of these techniques and approximations in combination with the generation of correlated wavefunctions *via* the DFT/MRCI approach makes it possible to compute spin-orbit coupling in organic molecules efficiently and with high confidence.

3 Technical details

Geometry optimizations of the six local minima (A) - (F) on the electronic ground state surface were performed for a restricted closed shell KS determinant. Herein, all atoms were constrained to lie in a common plane, thus imposing C_s symmetry. In all cases, the BH-LYP density functional was employed [11,12]. In addition, we have optimized the geometries of three low-lying triplet states by means of an unrestricted open-shell density functional theory procedure. It has to be noted in this context that the order of the triplet states is reversed with respect to the singlet states: T_1 has the same electronic structure as S_2 whereas T_2 closely resembles S_1. Starting from the DFT optimized structures, the geometries of the three lowest-lying singlets (S_0, S_1, and S_2) as well as the two lowest-lying triplets (T_1 and T_2) were refined at the DFT/MRCI level.

We tested three different basis sets: the standard TZVP and TZVPP basis sets from the Turbomole library [13,24] and a basis set, which we will call TZVPP+Ryd, where we added $3s$, $3p$, and $1d$ primitive diffuse Gaussians with origin at a dummy center and exponents of 0.05, 0.02, 0.008 (s and p Rydberg) and 0.015 (d Rydberg). The position of this dummy center was allowed to adjust in the geometry optimizations. It coincides approximately with the molecular center of mass. A numerical grid, usually employed for the cesium atom, was chosen for the quadrature of the exchange correlation at the dummy center. It turned out that the addition of a second polarization function (TZVPP) had almost no effect on the DFT/MRCI results. Further, excitation energies of the low-lying states were not altered upon augmentation of the basis set by Rydberg functions. On these grounds, we performed all geometry optimizations utilizing the TZVP basis. Further, the relative energetic location of the low-lying states of conformers (A) - (F) and the spin-orbit coupling between singlet and triplet states were determined in this basis. On the other hand, excitation energies and wavefunction characteristics of higher-lying electronic states are considerably affected by the inclusion of diffuse functions due to valence-Rydberg mixing. For the diketo tautomer (A), a vertical spectrum was calculated both in the TZVP and the TZVPP+Ryd bases.

A common set of molecular KS orbitals, optimized for the dominant closed shell determinant of the electronic ground state, was employed as a one-particle basis for the subsequent MRCI runs. In the latter step, all 42 valence electrons of uracil were correlated. In the TZVP basis, the MRCI space was spanned by energy-selected single and double excitations from approximately 70 reference CSFs. In each irreducible representation, eigenvalues and eigenvectors of six singlet and triplet states were determined. The reference space of the MRCI calculations in the TZVPP+Rydberg basis comprised approximately 130 CSFs for twelve roots in either spin and space symmetry.

The structure of the uracil-water complexes was determined without symmetry constraints. As it was not meant to explore a great part of the multi-minima potential energy hypersurface, we optimized just a single local minimum in each case, starting from a decently guessed nuclear arrangement. A TZVP basis was used throughout and all valence electrons on uracil and the water molecules were correlated. In the MRCI calculations, we computed the six lowest singlet and triplet states of each complex.

4 Results and discussion

4.1 The diketo form of uracil

4.1.1 The electronic ground state

The calculated equilibrium geometry of uracil in its diketo form is shown in Figure 2. Bond lengths in the six ring

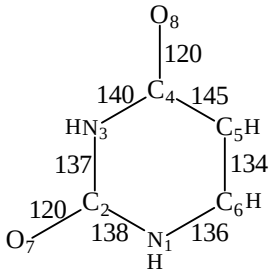

Fig. 2. Optimized geometry (DFT/MRCI, TZVP basis) of the diketo form (A) of uracil in its electronic ground state. All bond lengths are in pm units.

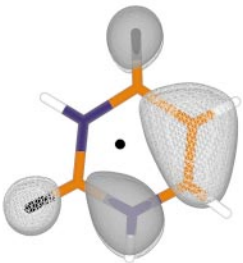

$(\pi_2),\ \epsilon = -0.3129 E_{\mathrm{H}}$

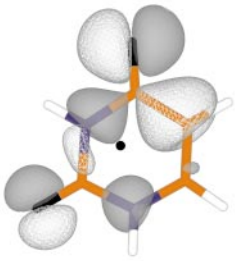

$(n_2),\ \epsilon = -0.3514 E_{\mathrm{H}}$

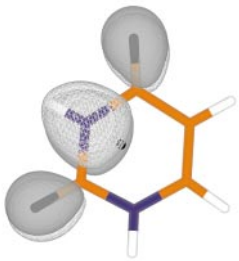

$(\pi_1),\ \epsilon = -0.3607 E_{\mathrm{H}}$

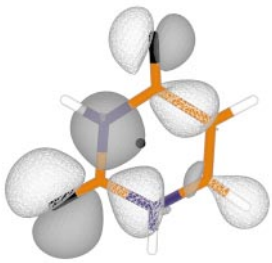

$(n_1),\ \epsilon = -0.3841 E_{\mathrm{H}}$

Fig. 3. The highest occupied n and π MOs. (Diketo form (A), S_0 geometry, TZVPP+Ryd basis, isoline = 0.020) The black dot in the six ring indicates the origin of the Rydberg basis.

agree excellently with experimental X-ray structural parameters [25]. Carbonyl bonds are slightly shorter than in the crystal structure (120 pm (both C–O groups, this work) *vs.* 121.5 pm (C_2–O_7) and 124.5 pm (C_4–O_8) [25]). We attribute parts of these differences to pairing effects in the solid state. Uracil crystals are built up from hydrogen bonded dimers in which the carbonyl oxygen O_8 is bonded to the N_3H group of the partner molecule thus leading to an elongation of the C_4–O_8 carbonyl bond. A trend in this direction is also seen in the uracil water complexes (see below) where the C–O bond distances are larger by 2–3 pm than in the isolated molecule.

Valence MOs that are important for an understanding of the spectrum are plotted in Figures 3 and 4. The highest occupied molecular orbital (HOMO, π_2) is a π-type orbital. It has a C_5–C_6 bonding character and is non-bonding elsewhere. The second highest MO (HOMO–1, n_2) is an in-plane orbital with large amplitudes for the O_8 carbonyl oxygen lone pair and the C_4–C_5 σ bond. The other oxygen lone pair, at O_7, dominates the n_1 orbital (HOMO–3). Finally, the third highest occupied MO (HOMO–2, π_1) has major contributions from the p_z orbitals on N_3 and both oxygen atoms. The lowest unoccupied MO (LUMO, π_3^*) exhibits a node between C_5 and C_6 whereas it is π bonding with respect to C_4–C_5. Further, it shows some C_4–O_8 anti-bonding characteristics. Several Rydberg orbitals are located in the energy gap between π_3^* and π_4^*, the next valence type MO. Like π_1, π_4^* is nearly C_{2v} symmetric with the second vertical reflection plane running through N_3 and C_6.

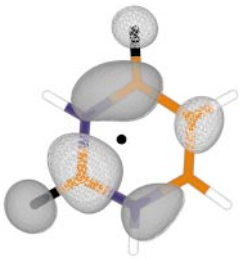

$(\pi_4^*),\ \epsilon = +0.0611 E_{\mathrm{H}}$

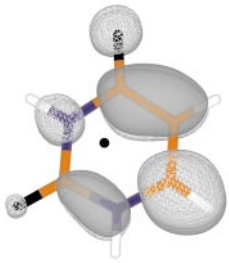

$(\pi_3^*),\ \epsilon = -0.0087 E_{\mathrm{H}}$

Fig. 4. The lowest unoccupied π^* MOs (other information as in Fig. 3).

4.1.2 Vertical absorption spectrum and characterization of excited states

Vertical singlet and triplet spectra of uracil were computed both in the TZVP and TZVPP+Ryd basis sets. As the results in Tables 1 and 2 suggest, the low-lying states (S_1, S_2, T_1, T_2, and T_3) are hardly influenced by the addition of further polarization functions and diffuse Gaussians. The first Rydberg excitations are found at 5.73 eV (triplet) and 5.83 eV (singlet). Energies and wavefunction characteristics of all states above 5.7 eV can therefore be trusted only if computed in basis sets augmented by Rydberg functions.

The first excited singlet state (S_1) is dominated by a single excitation from the second highest occupied MO (n_2, HOMO−1) to the lowest unoccupied MO (π_3^*, LUMO). The singlet-coupled $\pi_2 \rightarrow \pi_3^*$ (HOMO-LUMO) excitation yields the second excited singlet S_2. S_3 is of $^1A''$ symmetry. Its electronic structure corresponds to the promotion of an electron from the HOMO to the lowest a' orbital, which has Rydberg character at the ground state equilibrium geometry. Higher-lying singlets are considerably mixed. Dominant excitations occur into the valence π_3^* and π_4^* orbitals or into a variety of Rydberg orbitals that are globally labeled by R in Table 1.

As expected for ketones, $n \rightarrow \pi^*$ excitations are found to have negligible oscillator strengths for a dipole transition from the S_0 state. On the other hand, we obtain significant absorption probabilities for valence $\pi \rightarrow \pi^*$ excitations, in agreement with earlier theoretical treatments [8,9,27]. All strong transitions found in our calculated spectrum of uracil correspond to experimentally observed bands [1–4]. It has to be noted, however, that in polar solvents band maxima may shift considerably with respect to vapor spectra.

The first broad band in the vapor spectrum with a maximum at about 244 nm (5.08 eV) [2] is clearly due to

Table 1. Vertical singlet excitation energies ΔE [eV] and dipole transition oscillator strengths $f(r)$ of uracil in its diketo form.

State		HF/MRCI; RPA [8]		CASPT2 [9]		DFT/MRCI, present work				absorption
		DZVP+Ryd		TZVP+Ryd		TZVP	TZVPP+Ryd			maximum
		$\Delta E_{\rm MRCI}$	$\Delta E_{\rm RPA}$	ΔE	$f(r)$	ΔE	ΔE	$f(r)$	dominant excitation(s)	
S_0	$1^1A'$	0.00	0.00	0.00		0.00	0.00			
S_1	$1^1A''$	5.48	6.04	4.54	0.00	4.61	4.61	0.0002	$n_2 \rightarrow \pi_3^*$	4.68[a]
S_2	$2^1A'$	6.28	6.29	5.00	0.19	5.48	5.44	0.2626	$\pi_2 \rightarrow \pi_3^*$	5.08[b], 4.81[c], 4.77[d,e], 4.73[f]
S_3	$2^1A''$						5.83	0.0055	$\pi_2 \rightarrow R$	
S_4	$3^1A''$	7.15	7.32	6.00	0.00	(6.05)	5.95	0.0000	$n_2 \rightarrow \pi_4^*$, $n_1 \rightarrow \{\pi_3^*, \pi_4^*\}$	
S_5	$3^1A'$			5.81	0.08	(6.14)	6.15	0.0501	$\pi_1 \rightarrow \pi_3^*$	(6.05)[b], 6.05[e], 6.11[c], 6.14[d]
S_6	$4^1A'$			6.46	0.29	(6.79)	6.53	0.1565	$\pi_2 \rightarrow \{\pi_4^*, R\}$, $n_2 \rightarrow R$	6.63[b], 6.81[c]
S_7	$4^1A''$			6.37	0.00	(6.65)	6.57	0.0000	$n_1 \rightarrow \pi_3^*$, $n_2 \rightarrow \pi_4^*$	
S_8	$5^1A'$					(7.56)	6.65	0.0815	$n_2 \rightarrow R$, $\pi_2 \rightarrow \{R, \pi_4^*\}$	
S_9	$5^1A''$						6.71	0.0050	$\pi_2 \rightarrow R$	
S_{10}	$6^1A''$						6.76	0.0105	$\pi_2 \rightarrow R$	
S_{11}	$7^1A''$			6.95	0.00	(7.05)	6.85	0.0000	$n_2 \rightarrow \{\pi_4^*, R\}$	
S_{12}	$6^1A'$						7.07	0.0108	$\pi_2 \rightarrow R$	
S_{13}	$8^1A''$						7.09	0.0012	$\pi_1 \rightarrow R$	
S_{14}	$7^1A'$						7.17	0.0543	$n_2 \rightarrow R$	
S_{15}	$8^1A'$						7.29	0.0246	$n_1 \rightarrow R, n_2 \rightarrow R$	
S_{16}	$9^1A'$			7.01	0.76	(7.66)	7.39	0.5071	$\pi_1 \rightarrow \{\pi_4^*, R\}$, $n_2 \rightarrow R$	6.97[e]

[a] weak perpendicular transition in orthorhombic crystals of 1-methyluracil [26]; [b] vapor spectrum [2], (shoulder); [c] in trimethyl phosphate [2]; [d] in water [1]; [e] in water [4]; [f] in 2-methyltetrahydrofuran and ethanol/methanol [3].

Table 2. Vertical triplet excitation energies ΔE [eV] and dipole transition oscillator strengths $f(r)$ of uracil in its diketo form.

State		HF/MRCI [8]	DFT/MRCI, present work			
		DZVP+Ryd	TZVP	TZVPP+Ryd		
		ΔE	ΔE	ΔE	$f(r)$	dominant excitation(s)
T_1	$1^1A'$	4.00	3.68	3.68		$\pi_2 \rightarrow \pi_3^*$
T_2	$1^1A''$	5.30	4.40	4.39	0.0000	$n_2 \rightarrow \pi_3^*$
T_3	$2^1A'$	6.15	5.10	5.08	0.0061	$\pi_1 \rightarrow \pi_3^*$, $\pi_2 \rightarrow \pi_4^*$
T_4	$2^1A''$	6.94		5.73	0.0005	$\pi_2 \rightarrow R$
T_5	$3^1A'$	7.28	(5.85)	5.74	0.0139	$\pi_2 \rightarrow \pi_4^*$, $\pi_1 \rightarrow \{\pi_3^*, \pi_4^*\}$
T_6	$3^1A''$		(5.87)	5.76	0.0000	$n_2 \rightarrow \pi_4^*$, $n_1 \rightarrow \{\pi_3^*, \pi_4^*\}$
T_7	$4^1A'$		(6.39)	6.25	0.0155	$\pi_1 \rightarrow \{\pi_4^*, R, \pi_3^*\}$, $\pi_2 \rightarrow \pi_4^*$
T_8	$4^1A''$		(6.59)	6.50	0.0000	$n_1 \rightarrow \{\pi_3^*, \pi_4^*\}$
T_9	$5^1A'$			6.55	0.0000	$n_2 \rightarrow R$
T_{10}	$5^1A''$			6.63	0.0003	$\pi_2 \rightarrow R$
T_{11}	$6^1A''$			6.67	0.0000	$\pi_2 \rightarrow R$
T_{12}	$7^1A''$		(6.91)	6.73	0.0000	$n_1 \rightarrow \{\pi_4^*, R, \pi_3^*\}$, $n_2 \rightarrow \pi_3^*$
T_{13}	$6^1A'$			6.98	0.0021	$\pi_2 \rightarrow R$
T_{14}	$8^1A''$			7.01	0.0000	$\pi_1 \rightarrow R$
T_{15}	$7^1A'$			7.09	0.0000	$n_2 \rightarrow R$
T_{16}	$8^1A'$			7.19	0.0000	$n_1 \rightarrow R, n_2 \rightarrow R$
T_{17}	$9^1A'$		(7.41)	7.38	0.0911	$\pi_0 \rightarrow \pi_3^*$

the $S_0 \rightarrow S_2$ transition. Our best calculation (DFT/MRCI geometry, TZVPP+Ryd basis) poses the S_2 vertically at 5.44 eV. The band maximum experiences solvent shifts toward lower energies by up to 0.33 eV (compare Tab. 1). These trends are easily explained by the higher dipole moment of the S_2 state (5.59 D in the TZVPP+Ryd basis) compared to the ground state dipole moment (4.51 D) and the concomitant larger electrostatic interaction with the solvent. We attribute the shoulder at 205 nm (6.05 eV) [2] in the vapor spectrum to the weaker $S_0 \rightarrow S_5$ transition. In accord with the smaller dipole moment of the upper state (2.48 D), this band experiences a blue shift in polar solvents. For the next higher band system, measured at 187 nm (6.63 eV) [2] in the gas phase, a blue shift is reported in water. In this case, we find nearly equal dipole moments in the upper (S_6 4.06 D) and lower (S_0 4.51 D) states. However, the S_6 MRCI wavefunction has considerably large coefficients for $n_2 \rightarrow R$ excitations that are disadvantaged by hydrogen bonding (see below). The transition for which we find the largest dipole oscillator strength is $S_0 \rightarrow S_{16}$ at 7.39 eV. We believe that this excitation corresponds to the strong band at 177 nm (6.97 eV) reported by Callis for uracil in water [4]. A similar assignment was made by Lorentzon *et al.* [9]. As shown in Table 1, we find a valence-Rydberg mixed character for the S_{16} state. The most prominent valence configuration represents an excitation from the π_1 orbital to the virtual π_4^* orbital (see Figs. 3 and 4). Both orbitals are nearly symmetric with respect to an approximate vertical reflection plane and a two-fold rotation axis through N_3 and C_6. As already discussed by Lorentzon *et al.* [9], the large transition moment stems from a charge transfer from N_3 to the carbonyl groups.

The order of states is different in the triplet manifold where the $\pi_2 \rightarrow \pi_3^*$ excited state corresponds to T_1 and the triplet-coupled $n_2 \rightarrow \pi_3^*$ excitation to T_2 (Tab. 2). The third triplet state T_3 is a mixture of HOMO $\rightarrow$ LUMO+1 and HOMO$-2 \rightarrow$ LUMO excited configurations. It is located energetically well below a closely spaced group of triplets containing among others the first Rydberg state (T_4) in the triplet spectrum.

Most of our findings are in good agreement with experimental gas phase spectra and the results of previous CASPT2 calculations [2,9]. The largest deviation is found for the $S_0 \rightarrow S_2$ transition. If the band maximum is identified with the vertical excitation energy, our calculated value is too high by 0.35 eV. Our computed $S_0 \rightarrow S_5$ and $S_0 \rightarrow S_6$ vertical excitation energies, on the other hand, agree very well with experimental observations. Both correspond primarily to $\pi \rightarrow \pi^*$ excitations, *i.e.*, $\pi_1 \rightarrow \pi_3^*$ and $\pi_2 \rightarrow \pi_4^*$, respectively. It remains unclear at this point, why the first $\pi_2 \rightarrow \pi_3^*$ excitation ($S_0 \rightarrow S_2$) behaves differently. The energetic location of the Rydberg states was not determined at the CASPT2 level nor did the authors investigate the triplet states of uracil. Differences between the computed CASPT2 and DFT/MRCI excitation energies are found to be somewhat smaller for $n \rightarrow \pi^*$ states than for $\pi \rightarrow \pi^*$ states. The general good agreement between the computed DFT/MRCI spectrum and experiment found in this work are in accord with the results of Grimme and Waletzke [10]. In a series of DFT/MRCI calculations on 37 vertical transitions in mostly organic molecules, these authors obtained a root mean square deviation from experimental data of 0.15 eV, the largest error being -0.35 eV for an $n \rightarrow \pi^*$ transition in thioformaldehyde. Unscaled excitation energies from Hartree-Fock based MRCI and random phase approximation (RPA) calculations by Petke *et al.* [8] are considerably too high.

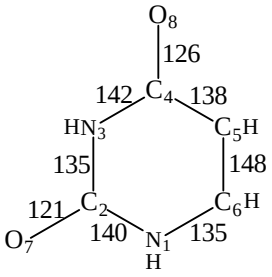

Fig. 5. Optimized geometry (DFT/MRCI, TZVP basis) of the second excited singlet state of uracil.

4.1.3 Geometries of excited states and vibrational fine structure

The observation of at least three vibrational quanta (spaced by $\approx$ 790 cm^{-1}) superimposed on the broad, otherwise featureless first band suggests a considerable change of geometry in the upper state [3]. A harmonic vibrational analysis of the S_0 equilibrium structure (at the DFT level) exhibits two modes in the desired energy range. Mode 11 at 798 cm^{-1} is an out-of-plane vibration of C_2 (the center of the N,N–C–O trihedron). Mode 12 at 802 cm^{-1} corresponds to an in-plane breathing vibration of the six ring. The computed frequency of mode 11 is in excellent agreement with a measured IR band for a C–O out-of-plane vibration at 806 cm^{-1} [28]. The intensity of mode 12 (4 km/mol) is probably too low for an experimental observation in the infrared.

Optimization of the S_2 state geometry without symmetry constraints at the DFT/MRCI level did not show any tendency for an S_2 minimum structure with a pyramidal N,N–C–O group. The most obvious change with respect to the S_0 molecular geometry is the breaking of the double bond between C_5 and C_6 (compare Figs. 2 and 5) and the shortening of the single bond between C_4 and C_5. These trends are consistent with the nuclear distortions in mode 12. Indeed, the central CH group (C_5 and the H linked to it) is the group with the largest displacement vector. From these results we conclude that the vibrational structure observed by Becker and Kogan in the first band system is due to a symmetric breathing mode of the six ring. This assignment is also consistent with a moderate change of the vibrational spacing for N,N-dimethyluracil (DMU) ($\approx$770 cm^{-1}) and a larger red shift for thymine, *i.e.*, 5-methyluracil with the methyl group replacing the hydrogen at C_5. Due to geometry relaxation, the energy of the S_2 state drops by approximately 0.5 eV yielding an adiabatic excitation of 4.99 eV in the TZVP

Table 3. Relative energies ΔE [eV] of uracil in the diketo tautomeric form at various molecular geometries (DFT/MRCI, TZVP basis). The nomenclature S_0, S_1, S_2, T_1, T_2, and T_4 follows the order of states at the ground state equilibrium geometry.

State	S_0 geometry	S_1 geometry $n \to \pi^*$	S_2 geometry $\pi \to \pi^*$	T_1 geometry $\pi \to \pi^*$	T_2 geometry $n \to \pi^*$	T_4 geometry[a] $\pi \to \sigma^*$
S_0, $1^1A'$	0.00	0.59	0.63	0.47	0.52	5.84
S_1, $1^1A''$	4.61	3.96	4.30	4.41	3.96	4.11
S_2, $2^1A'$	5.48	5.21	4.99	5.10	5.23	5.88
T_1, $1^3A'$	3.68	3.51	3.29	3.20	3.52	6.09
T_2, $1^3A''$	4.40	3.84	4.22	4.32	3.83	4.97
T_3, $2^3A'$	5.10	4.72	4.99	5.04	4.73	6.52

[a] optimized at the UDFT level.

Table 4. Dipole moments μ [D] of uracil in the diketo tautomeric form at the ground state geometry and at the equilibrium geometry of the respective state (DFT/MRCI, TZVP basis).

State	S_0 geometry	equilibrium geometry
S_0, $1^1A'$	4.58	4.58
S_1, $1^1A''$	2.54	2.98
S_2, $2^1A'$	5.85	5.11
T_1, $1^3A'$	3.89	3.75
T_2, $1^3A''$	2.67	3.02

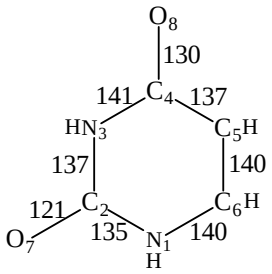

Fig. 6. Optimized geometry (DFT/MRCI, TZVP basis) of the first excited singlet state of uracil.

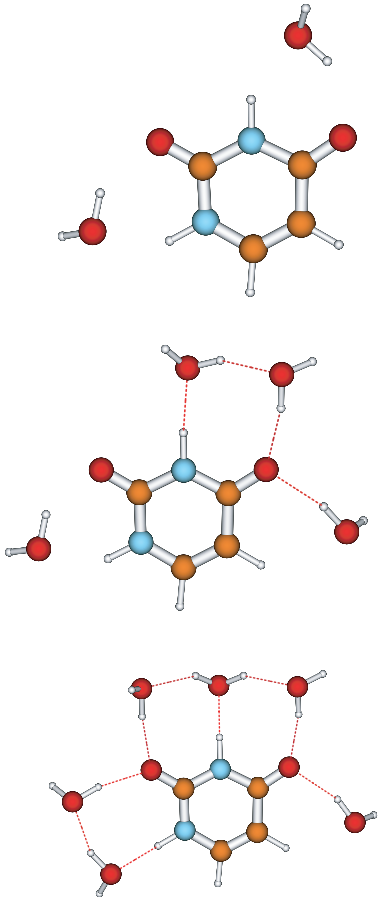

Fig. 7. Optimized geometries (DFT, TZVP basis) of uracil-water complexes.

basis. Emission from the S_2 state is predicted to occur at 4.36 eV because the molecule retains the S_2 geometry for a short period of time also in the S_0 state (see Tab. 3).

Weak fluorescence was observed at 300 nm (4.13 eV) for uracil and DMU in a hydroxylic solvent (ethanol-methanol) and attributed to an $n \to \pi^*$ transition [3]. In 2-MTHF, only DMU shows fluorescence whereas uracil phosphorescences. The $n_2 \to \pi_3^*$ excitation leads to a considerable lengthening of the C_4–O_8 carbonyl bond and the formation of a double bond between C_4 and C_5 (Fig. 6). An adiabatic excitation energy of 3.95 eV (compared to 4.61 eV in absorption and 3.36 eV in emission) is obtained for S_1.

The S_1 state exhibits a much smaller dipole moment than the S_0 ground state (Tab. 3), and will experience a blue shift in polar media whereas S_2 is lowered. Moreover, hydrogen bonding is supposed to favor electronic states with doubly occupied n_1 and n_2 orbitals because these orbitals exhibit considerable lone-pair character at the carbonyl oxygens (Fig. 3). In a polar protic solvent, hydrogen bonding will therefore enforce the blue shift of the S_1 excitation energy, thus reducing the energy gap between S_1 and S_2 further. These assumptions are verified by the trends found for various uracil water complexes sketched in Figure 7. Interestingly, we find the largest effects for uracil·$4H_2O$, probably due to the asymmetric arrangement of the water molecules. (In the starting geometry, each water molecule was bonded to a single N or O atom. The asymmetric arrangement is caused by collaborative reinforcement of the hydrogen bonds.) As shown

Table 5. Excitation energies ΔE [eV] of low-lying electronic states in isolated uracil molecules compared with uracil-water complexes. All geometries were optimized at the DFT level.

	State	DFT/MRCI, TZVP basis			
		uracil	uracil·2H_2O	uracil·4H_2O	uracil·6H_2O
S_1	$^1(n_2 \rightarrow \pi_3^*)$	4.68	4.91	5.13	5.07
S_2	$^1(\pi_2 \rightarrow \pi_3^*)$	5.55	5.44	5.33	5.43
T_1	$^3(\pi_2 \rightarrow \pi_3^*)$	3.77	3.78	3.77	3.83
T_2	$^3(n_2 \rightarrow \pi_3^*)$	4.45	4.70	4.94	4.87
T_3	$^3(\pi_1 \rightarrow \pi_3^*, \pi_2 \rightarrow \pi_4^*)$	5.16	5.14	5.13	5.12

in Table 5, the $n \rightarrow \pi^*$ excited states (S_1 and T_2) are significantly raised in energy in hydrogen bonded complexes with respect to the ground state and $\pi \rightarrow \pi^*$ excitations. Oscillator strengths for a dipole transition to the electronic ground state remain nearly constant upon complexation with water molecules. In conclusion, energy considerations argue for S_1 as the origin of the 300 nm fluorescence. The computed oscillator strength of the vertical transition amounts to merely 4×10^{-5} at this point on the potential hypersurface, however [3].

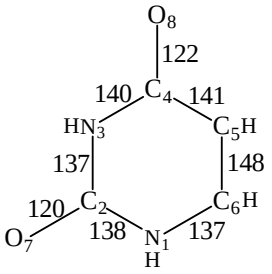

Fig. 8. Optimized geometry (DFT/MRCI, TZVP basis) of the first excited triplet state of uracil.

Surprising results are obtained if one optimizes the geometry of another A'' open shell configuration (T_4 and S_3 in the vertical spectrum) where a hole has been created in π_2 and a particle in the lowest unoccupied a' symmetric orbital. As mentioned before, this orbital has predominantly Rydberg character at the S_0 equilibrium geometry. When the geometry of the triplet state is relaxed, the a' orbital gains more and more valence character and eventually turns into a σ_{NH}^* antibonding orbital. As a consequence, uracil loses the hydrogen atom linked to N_1. (In nucleic acids, this particular photochemical bond cleavage will not occur as uracil is linked to the RNA backbone at the N_1 position.) At large N_1–H distances, the lowest electronic state is a singlet of $^1A''$ symmetry. In addition to the dominant $\pi_2 \rightarrow \sigma_{NH}^*$ configuration, the wavefunction has large coefficients for double excitations, the most important being $\sigma_{NH}\pi_2 \rightarrow \sigma_{NH}^{*2}$. At the T_4 optimized geometry (with an N–H distance of roughly 400 pm), $1^1A''$ is located ≈4.1 eV above the diketo minimum on the S_0 potential energy hypersurface and only marginally above the $^1A''$ ($n_2 \rightarrow \pi_3^*$) S_1 minimum. The corresponding triplet state is higher in energy (at ≈5.0 eV). Both A'' states are located significantly below the first $^1A'$ state (≈5.8 eV) that correlates with the the diketo (A) ground state configuration. These results are noteworthy, because they suggest the existence of a flat potential well on the singlet hypersurface close to the dissociation continuum. Further, they imply that various intersections of potential energy hypersurfaces occur in the energy regime of the $\pi_2 \rightarrow \pi_3^*$ absorption. At present, we do not have a computer code for a systematic search of potential hypersurface crossings. Without having properly located the seam or point of intersection between $^1(\pi_2 \rightarrow \sigma^*)$ and the other singlet states, all discussion about predissociation or a fast relaxation to the electronic ground state being the cause for the diffuseness of the absorption spectrum must remain speculative, of course. Nevertheless, our results strongly point towards a participation of the $^1(\pi_2 \rightarrow \sigma_{NH}^*)$ excited state in the depletion of the $^1(\pi_2 \rightarrow \pi_3^*)$ population[1].

4.1.4 Spin-orbit coupling and phosphorescence

A broad phosphorescence band with maximum at 450 nm (2.76 eV) was observed by Becker and Kogan [3] at 77 K for uracil in 2-MTHF, a polar aprotic solvent. It is quenched upon N,N-dimethyl substitution or in a hydroxylic solvent. In the latter cases, fluorescence is found instead. The triplet state lifetime was not determined for the uracil molecule. A rough estimate can be obtained from measurements of the corresponding transition in thymine, however. For thymine, Becker and Kogan observe a total triplet lifetime of $\tau_P^{obs} = 75$ ms at 77 K in 2-MTHF from which they derive a phosphorescence lifetime of $\tau_P^0 \approx 0.7$ s [3]. This weak phosphorescence was assigned as $^3(\pi \leftarrow \pi^*)$ transition by these scientists.

From an energetic point of view, this assignment is in good agreement with our calculations: at the T_1 equilibrium geometry (sketched in Fig. 8), the computed vertical deexcitation energy of the isolated molecule amounts to ≈2.73 eV (see Tab. 3). Adiabatically, T_1 is located about 3.20 eV above S_0. For phosphorescence in an organic molecule to be large, two scenarios can be thought of [30,31]:

1. the triplet state interacts strongly *via* spin-orbit coupling with an excited singlet state that in turn has a large dipole transition moment to the singlet ground state;
2. the triplet state has a large spin-orbit matrix element with the singlet ground state and the (static) dipole moments differ considerably between the two.

[1] After submission of this work we became aware of an article discussing the role of singlet $\pi\sigma^*$ states in photochemical hydrogen detachment and hydrogen transfer reactions [29].

Table 6. Spin-orbit matrix elements (absolute values) [cm^{-1}] of the lowest singlet and triplet states in the diketo (A) form of uracil, calculated at the T_1 geometry. The component of the spin-orbit Hamiltonian is indicated in parentheses.

$\langle T_1(A')\|\mathcal{H}_{SO}\|S_0(A')\rangle$	$0.008(z)$
$\langle T_1(A')\|\mathcal{H}_{SO}\|S_1(A'')\rangle$	$0.510(x)/33.523(y)$
$\langle T_1(A')\|\mathcal{H}_{SO}\|S_2(A')\rangle$	$0.024(z)$
$\langle T_2(A'')\|\mathcal{H}_{SO}\|S_0(A')\rangle$	$9.157(x)/42.805(y)$
$\langle T_2(A'')\|\mathcal{H}_{SO}\|S_1(A'')\rangle$	$0.215(z)$
$\langle T_2(A'')\|\mathcal{H}_{SO}\|S_2(A')\rangle$	$2.936(x)/23.370(y)$
$\langle T_2(A'')\|\mathcal{H}_{SO}\|T_1(A')\rangle$	$0.402(x)/30.874(y)$
$\langle T_3(A')\|\mathcal{H}_{SO}\|S_0(A')\rangle$	$0.001(z)$
$\langle T_3(A')\|\mathcal{H}_{SO}\|S_1(A'')\rangle$	$2.870(x)/31.610(y)$
$\langle T_3(A')\|\mathcal{H}_{SO}\|S_2(A')\rangle$	$0.019(z)$
$\langle T_3(A')\|\mathcal{H}_{SO}\|T_1(A')\rangle$	$0.020(z)$
$\langle T_3(A')\|\mathcal{H}_{SO}\|T_2(A'')\rangle$	$2.616(x)/32.428(y)$

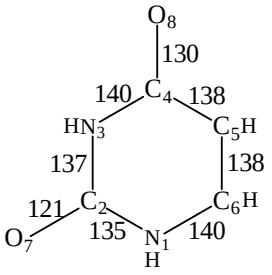

Fig. 9. Optimized geometry (DFT/MRCI, TZVP basis) of the second excited triplet state of uracil.

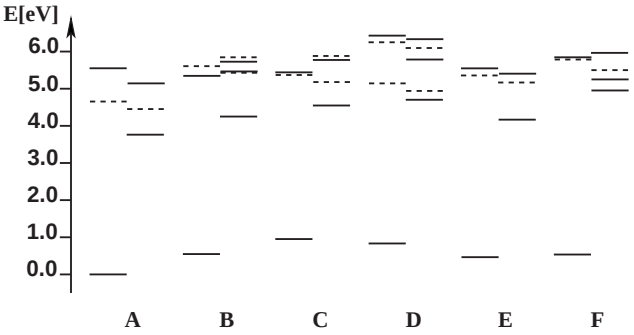

Fig. 10. Relative DFT/MRCI energies (TZVP basis) of low-lying electronic states for various tautomers of uracil: diketo (A), ketoenol (B)–(E), dienol (F) (*cf.* Fig. 1). Solid lines denote states of A' symmetry, dashed lines A'' states. For each tautomer, singlets are shown to the left, triplets to the right.

Neither condition is fulfilled by the T_1 state of uracil. In Table 6, spin-orbit matrix elements between the low-lying electronic states of uracil are listed. Spin-orbit interaction is very weak between T_1 and A' symmetric singlets, *i.e.*, $\pi \rightarrow \pi^*$excitations that have high probabilities for a dipole transition to the ground state. This applies equally to matrix elements with energetically higher A' states, not shown in the table. The direct spin-orbit interaction between T_1 and S_0 is negligibly small, too. On the other hand, significant spin-orbit interaction with the A'' states ($n \rightarrow \pi^*$) is found, the latter having only marginal radiative transition probabilities to S_0. Employing spin-orbit matrix elements, dipole transition moments, and excitation energies as computed at the T_1 geometry, we calculate the high-temperature limit for the T_1 phosphorescence lifetime to be $\tau_P^0 \approx 7.5$ s. These results are in agreement with qualitative considerations about phosphorescence rates of $^3(\pi \rightarrow \pi^*)$ states in organic molecules [32]. Further, rates for inter-system crossing (ISC) between S_2 and T_1 are predicted to be very small. T_1 will therefore not be populated directly *via* the strong $S_0 \rightarrow S_2$ absorption. Indirectly, T_1 may be reached from the S_2 state either by internal conversion (IC) from S_2 to S_1 and subsequent ISC to T_1 or by ISC between S_2 and T_2 and IC within the triplet moiety.

The T_2 state, by contrast, exhibits an important direct spin-orbit coupling matrix element with the S_0 electronic ground state (Tab. 6) and their dipole moments differ considerably (Tab. 3). Moreover, its spin-orbit interaction with the close-lying S_2 state lends intensity to the phosphorescence and enables the effective population of T_2 *via* ISC after absorption. Accordingly, our calculations predict a much smaller radiative lifetime for T_2 ($\tau_P^0 \approx 1$ ms). On the other hand, the large spin-orbit coupling between T_2 and the lower-lying T_1 and S_0 states will lead to a rapid non-radiative decay of the T_2 state, if vibrational overlap is sufficient. At the T_2 optimized geometry (Fig. 9), the energy gap between T_2 and S_0 amounts to approximately 3.3 eV which is still quite a lot, whereas the energy difference between T_2 and T_1 is only 0.3 eV. All of these facts support the assumption that the radiative and non-radiative depletion of the T_2 is fast.

4.2 Other tautomeric forms of uracil

4.2.1 Relative stabilities of ground and excited states

Relative energies of the electronic ground states and low-lying excited states of the six tautomeric forms (A-F) of uracil are sketched in Figure 10. In accord with experiment, the diketo form (A) is found to represent the global minimum on the ground state potential energy surface. Next in energetic order come the ketoenol forms (B) and (E) and the dienol tautomer (F). They are predicted to have very similar ground state energies in the gas phase, approximately 0.5 eV above the diketo minimum. Estimating solvent effects on the basis of dipole moment differences (Tab. 7), it can be assumed that tautomer (B) is stabilized relative to the diketo form by a polar solvent whereas (E) and (F) will be destabilized. The ketoenol forms (C) and (D) are those with the largest dipole moments and least favorite energies in vacuo. Similar trends have been obtained earlier by AM1 calculations [33,34].

The first excited triplet state ($\pi \rightarrow \pi^*$ in all tautomers) follows roughly the energetic trend of the electronic ground state, with the exception of the dienol form (F) where T_1 is considerably blue shifted. No such

Table 7. Relative DFT/MRCI energies, dipole moments (TZVP basis) and oscillator strengths of uracil in various tautomeric forms: diketo (A), ketoenol (B)–(E), dienol (F). Ground state geometries were optimized at the DFT level. For structure codes, see Figure 1.

tautomer		$1^1A'(S0)$		$1^1A''(n \rightarrow \pi^*)$			$2^1A'(\pi \rightarrow \pi^*)$		
		ΔE [eV]	μ [D]	ΔE [eV]	μ [D]	$f(r)$	ΔE [eV]	μ [D]	$f(r)$
diketo	(A)	0.00	4.53	4.68	2.53	0.2×10^{-3}	5.55	5.88	0.277
ketoenol	(B)	0.54	4.98	5.62	1.10	1.2×10^{-3}	5.34	3.68	0.110
ketoenol	(C)	0.95	7.33	5.49	4.25	3.6×10^{-3}	5.55	2.55	0.179
ketoenol	(D)	0.83	6.47	5.17	2.11	0.7×10^{-4}	6.43	5.14	0.095
ketoenol	(E)	0.47	3.23	5.36	2.26	0.3×10^{-3}	5.55	3.04	0.223
dienol	(F)	0.52	1.35	5.82	1.96	9.9×10^{-3}	5.85	0.82	0.113

trends can be made out for the other low-lying excited electronic states. Even their relative order varies from tautomer to tautomer. Oscillator strengths are found to be very small for all $n_2 \rightarrow \pi_3^*$ excitations. The observation of strong fluorescence from an $n \rightarrow \pi^*$ excited state in a ketoenol tautomeric form of uracil, as reported by Ito and coworkers [5,6], appears thus extremely improbable. In contrast, the $\pi \rightarrow \pi^*$ excited $2\ ^1A'$ state is connected to S_0 by a reasonable dipole transition probability in all tautomers.

4.2.2 The ketoenol tautomer (B)

Among all non-diketo tautomers, ketoenol (B) is the most interesting one: besides (A) and the higher lying form (D), it is the only tautomer that can occur in nucleic acids. Furthermore, the order of the $n \rightarrow \pi^*$ and $\pi \rightarrow \pi^*$ excited singlet states is reversed compared to their order in the diketo form, *i.e.*, $2^1A'$ represents the S_1 state in tautomer (B). This fact shows that the $2^1A'$ ($\pi \rightarrow \pi^*$) and $1^1A''$ ($n \rightarrow \pi^*$) potential energy surfaces must intersect somewhere. A geometry optimization of the T_1 state in the ketoenol form (B) leads to the lowest point on the $2^1A'$ hypersurface detected so far, merely 4.99 eV above the diketo ground state or 4.45 eV above the local minimum of form (B). The calculated oscillator strength for a dipole transition from $S_0 \rightarrow S_1$ should be sufficient for an experimental observation in absorption.

Whether it will be possible to observe fluorescence from this state will critically depend on the solvent. We predict the S_1 and T_2 states of tautomer (B) to be nearly degenerate in the gas phase. The electronic spin-orbit coupling matrix element between these states is not very large (see Tab. 8), but appears to be sufficient for a rapid inter-system crossing between states with nearly zero energy gap. In a polar solvent, S_1 should drop significantly below T_2 because of its higher dipole moment (3.68 D (S_1) *vs.* 0.27 D (T_2)) precluding a non-radiative spin-forbidden transition from S_1 to T_2. Complexation with water molecules in the gas phase ought to have a similar effect on the energy gap between S_1 to T_2. Spin-orbit coupling to the lower-lying T_1 state is not efficient either because of a nearly vanishing electronic interaction matrix element and small vibrational overlap. In a polar surrounding or in hydrogen-bonded complexes, the S_1 ($\pi \rightarrow \pi^*$) state might therefore show fluorescence in the ketoenol tautomeric form (B), if the latter can be synthesized.

Table 8. Spin-orbit matrix elements (absolute values) [cm^{-1}] of the lowest singlet and triplet states in the ketoenol (B) forms of uracil at the ground state equilibrium geometry. The component of the spin-orbit Hamiltonian is indicated in parentheses. Note that the order of singlet states is reversed with respect to tautomer (A).

$\langle T_1(A')\|\mathcal{H}_{SO}\|S_0(A')\rangle$	$0.04(z)$
$\langle T_1(A')\|\mathcal{H}_{SO}\|S_2(A'')\rangle$	$8.15(x)/16.08(y)$
$\langle T_1(A')\|\mathcal{H}_{SO}\|S_1(A')\rangle$	$0.00(z)$
$\langle T_2(A'')\|\mathcal{H}_{SO}\|S_0(A')\rangle$	$4.69(x)/1.60(y)$
$\langle T_2(A'')\|\mathcal{H}_{SO}\|S_2(A'')\rangle$	$2.82(z)$
$\langle T_2(A'')\|\mathcal{H}_{SO}\|S_1(A')\rangle$	$5.04(x)/1.00(y)$
$\langle T_2(A'')\|\mathcal{H}_{SO}\|T_1(A')\rangle$	$2.08(x)/0.27(y)$
$\langle T_3(A')\|\mathcal{H}_{SO}\|S_0(A')\rangle$	$0.00(z)$
$\langle T_3(A')\|\mathcal{H}_{SO}\|S_2(A'')\rangle$	$8.39(x)/1.44(y)$
$\langle T_3(A')\|\mathcal{H}_{SO}\|S_1(A')\rangle$	$0.01(z)$
$\langle T_3(A')\|\mathcal{H}_{SO}\|T_1(A')\rangle$	$0.01(z)$
$\langle T_3(A')\|\mathcal{H}_{SO}\|T_2(A'')\rangle$	$4.50(x)/2.57(y)$

5 Conclusions

In this work, we have investigated the singlet and triplet spectra of several uracil tautomers by quantum chemical methods. The most stable nuclear arrangement corresponds to the diketo form of uracil, the electronic ground state of other tautomers being approximately 0.5–1 eV higher in energy. Our calculations yield large oscillator strengths for $\pi \rightarrow \pi^*$ excitations, in agreement with earlier theoretical and experimental studies. Rydberg and $n \rightarrow \pi^*$ states exhibit very small probabilities for a dipole transition from or to the electronic ground state. The lowest lying excited state corresponds to a $^3(\pi \rightarrow \pi^*)$ excitation, followed by a triplet coupled $n \rightarrow \pi^*$ state. The order of states is reversed in the singlet spectrum of the diketo form. The results of the present theoretical investigation show that the first dark $^1(n \rightarrow \pi^*)$ S_1 and the $^1(\pi \rightarrow \pi^*)$

S_2 state, into which absorption is observed, are close in energy at the S_2 equilibrium geometry. The energy gap between these states is even diminished in a polar surrounding and due to hydrogen bonding. The proximity of dark and absorbing states may be one reason for the diffuseness of the uracil absorption bands. Our calculations indicate that also a dissociative A'' state in which a σ^*_{NH} antibonding orbital is occupied might play a decisive role.

The vibrational structure in the first broad band with a spacing of ≈ 790 cm^{-1} has been identified to stem from a breathing vibration of the uracil six ring. A carbonyl out-of-plane vibrational mode exhibits nearly the same frequency. The question whether the latter mode leads to vibronic interaction between the S_1 and S_2 state can presently not be answered with high confidence and must remain speculation for the time being.

Spin-orbit mean-field calculations yield large coupling matrix elements between A' and A'' electronic states. By contrast, the interaction between singlets and triplets of the same spatial symmetry is negligible. Calculated phosphorescence lifetimes support the assumption that the phosphorescence, measured in 2-methyl-tetrahydrofuran after $S_0 \rightarrow S_2$ $^1(\pi \rightarrow \pi^*)$ absorption, stems from the $^3(\pi \rightarrow \pi^*)$ T_1 state.

Funding by the Deutsche Forschungsgemeinschaft (DFG) through project Ma 1051/5-1 is gratefully acknowledged. It is a pleasure to thank Stefan Grimme (Münster) and Mirko Waletzke for making their DFT/MRCI code available to us. Thanks are also due to Rainer Weinkauf (Düsseldorf) for valuable discussions and to Marcus Gastreich (FhG-SCAI, St. Augustin) for technical assistance with the molecular orbital plots.

References

1. D.R. Voet, W.B. Gratzer, R.A. Cox, P. Doty, Biopolymers **1**, 193 (1963)
2. L.B. Clark, G.G. Peschel, I. Tinoco Jr, J. Phys. Chem. **69**, 3615 (1965)
3. R. Becker, G. Kogan, Photochem. Photobiol. **31**, 5 (1980)
4. P.R. Callis, Annu. Rev. Phys. Chem. **34**, 329 (1983)
5. M. Fujii, T. Tamura, N. Mikami, M. Ito, Phys. Chem. Lett. **126**, 583 (1986)
6. Y. Tsuchiya, T. Tamura, M. Fujii, M. Ito, J. Phys. Chem. **92**, 1760 (1988)
7. B.B. Brady, L.A. Peteanu, D.H. Levy, Chem. Phys. Lett. **147**, 538 (1988)
8. J.D. Petke, G.M. Maggiora, R.E. Christoffersen, J. Phys. Chem. **96**, 6992 (1992)
9. J. Lorentzon, M.P. Fülscher, B.O. Roos, J. Am. Chem. Soc. **117**, 9265 (1995)
10. S. Grimme, M. Waletzke, J. Chem. Phys. **111**, 5645 (1999)
11. A.D. Becke, J. Chem. Phys. **98**, 1372 (1993)
12. C. Lee, W. Yang, R.G. Parr, Phys. Rev. B **37**, 785 (1988)
13. R. Ahlrichs, M. Bär, M. Häser, H. Horn, C. Kölmel, Chem. Phys. Lett. **162**, 165 (1989)
14. O. Treutler, R. Ahlrichs, J. Chem. Phys. **102**, 346 (1995)
15. O. Vahtras, J. Almlöf, M.W. Feyereisen, Chem. Phys. Lett. **213**, 514 (1993)
16. F. Weigend, M. Häser, H. Patzelt, R. Ahlrichs, Chem. Phys. Lett. **294**, 143 (1998)
17. K. Eichkorn, O. Treutler, H. Öhm, M. Häser, R. Ahlrichs, Chem. Phys. Lett. **240**, 283 (1995)
18. F Schneider, *Entwicklung eines Treibers zur numerischen Bestimmung von Minima auf CI-Potenzialflächen und Anwendung auf angeregte Elektronenzustände des Uracil-Moleküls*, diploma thesis, University of Bonn available through: `http://www.theochem.uni-duesseldorf.de` (2002)
19. M. Kleinschmidt, J. Tatchen, C.M. Marian, J. Comp. Chem. **23**, 824 (2002)
20. B.A. Heß, C.M. Marian, U. Wahlgren, O. Gropen, Chem. Phys. Lett. **251**, 365 (1996)
21. J. Tatchen, C.M. Marian, Chem. Phys. Lett. **313**, 351 (1999)
22. D. Danovich, C.M. Marian, T. Neuheuser, S.D. Peyerimhoff, S. Shaik, J. Phys. Chem. A **102**, 5923 (1998)
23. Amfi is an atomic spin-orbit integral program written by B. Schimmelpfennig, University of Stockholm, 1996
24. A. Schäfer, C. Huber, R. Ahlrichs, J. Chem. Phys. **100**, 5829 (1994)
25. R.F. Steward, L.H. Jensen, Acta Chrystallogr. **23**, 1102 (1967)
26. W.A. Eaton, T.P. Lewis, J. Chem. Phys. **53**, 2164 (1970)
27. A. Broo, A. Holmén, J. Phys. Chem. **101**, 3589 (1997)
28. M. Szczesniak, M.J. Novak, H. Rostkowska, K. Szczesniak, J. Am. Chem. Soc. **105**, 5969 (1983)
29. A.L. Sobolewski, W. Domcke, C. Dedonder-Lardeux, C. Jouvet, Phys. Chem. Chem. Phys. **4**, 1093 (2002)
30. C.M. Marian, Spin-orbit coupling in molecules, in *Reviews In Computational Chemistry*, edited by K. Lipkowitz, D. Boyd (Wiley-VCH, Weinheim, 2001), Vol. 17, pp. 99–204
31. J. Tatchen, M. Waletzke, C.M. Marian, S. Grimme, Chem. Phys. **264**, 245 (2001)
32. N.J. Turro, *Modern Molecular Photochemistry* (University Science Books, Sausalito, CA, 1991)
33. U. Norinder, J. Mol. Struct. (Theochem) **151**, 259 (1987)
34. A.R. Katritzky, M. Karelson, J. Am. Chem. Soc. **113**, 1561 (1991)